Physics modeling of storms and substorms with solar wind data

W. Horton, M. L. Mays, and E. Spencer

Abstract: Analytic solar wind signals are constructed using data from the ACE satellitefor the 3-6 October 2000 and 15-24 April 2002 geomagnetic storm events which included interplanetary shocks and magnetic clouds. The response of the WINDMI model, an eight dimensional model of the solar wind driven magnetosphere-ionosphere system, to the analytic signals was examined for these events. The role of the shocks are examined by using analytic signals in which the shock feature in the density, solar wind velocity, and magnetic field magnitude are tested individually. During the 3-6 October 2000 event, the shock near the end of the 42 hr magnetic cloud is shown to be largely responsible for the very large region 1 field aligned current surges associated with the $-AL > 1300$nT peaks at the end of the main phase of the storm. Real-time WINDMI is being tried as a prediction tool and we briefly describe the first results in the new mode. Real-time data from ACE is used and provides a prediction for the AL and Dst about 1-2 hours before the data is available for these indices. We show WINDMI real-time predictions that were captured for a recent storm in 14-15 April 2006.

Key words: Substorms, Modeling.

1. Introduction

Interplanetary coronal mass ejections (ICMEs) are the interplanetary counterparts of coronal mass ejections (CMEs) at the Sun and are observed as enhanced magnetic structures in the solar wind lasting on the order of a day [7]. Magnetic clouds (MCs) are a subclass of ICMEs with above-average strength magnetic fields which rotate smoothly through a large angle in a low beta plasma [1]. Earth-directed Halo ICMEs often trigger geomagnetic storms such as the storms of 3-6 October 2000 and 15-24 April 2002. Interplanetary (IP) shocks and their resulting geomagnetic activity are usually caused by Halo CMEs [6–8]. Solar wind velocity and magnetic field strength variation across interplanetary shocks are correlated with the Dst index [3]. In addition multiple interplanetary magnetic structures are more geoeffective than single interplanetary magnetic structures [4].

In order to understand the effect of IP shocks and MCs on geomagnetic activity, we use the WINDMI model which takes driving voltage derived from Advanced Composition Explorer (ACE) satellite data as input and outputs a predicted westward auroral electrojet index (AL) and equatorial disturbance storm time index (Dst). We construct analytic solar wind signals from ACE data for the 3-6 October 2000 event and derive an analytic input driving voltage. The role of the shocks are examined by removing the shock features individually from each analytic parameter: density, solar wind velocity, and magnetic field magnitude, then examing the change in the WINDMI output of AL and Dst.

The WINDMI model is decribed in section 2. The analysis of the shock events in the 3-6 October 2000 storm presented in section 2.1 and the 15-24 April 2002 storm in section 2.2. The new real-time WINDMI model is discussed in section 3.

Received 15 May 2006.

W. Horton, M. L. Mays, and E. Spencer. Institute for Fusion Studies, University of Texas at Austin, Austin, Texas, USA.

2. WINDMI Model Description

The WINDMI model solves eight coupled ODE's for current, velocity, and pressure in the solar wind driven magnetosphere-ionosphere system. The model is explained in detail in [9] and [10]. WINDMI has ring current energization from substorm injections and therefore outputs a predicted westward auroral electrojet index (AL) and equatorial disturbance storm time index (Dst).

Complete measurements of solar wind proton density, solar wind velocity and the Interplanetary Magnetic Field (IMF) in GSM coordinates for the two geomagnetic storm periods are available from the Advance Composition Explorer (ACE) satellite. We use these quantities to derive the input dynamo driving voltage for the WINDMI model. The dynamo driving voltage $V_{sw}(t)$ was calculated from the analytic data using a formula given by *Siscoe et al.* [19], [18], and [17] for the coupling of the solar wind to the magnetopause using the solar wind dynamic pressure P_{sw} to determine the standoff distance. The formula for V_{sw} is given by,

$$V_{sw}(kV) = 30.0(kV) + 57.6E_{sw}(mV/m)P_{sw}^{-1/6}(nPa) \quad (1)$$

where $E_{sw} = v_{sw}(B_y^2 + B_z^2)^{1/2}\sin(\frac{\theta}{2})$ is the solar wind electric field with respect to the magnetosphere and the dynamic solar wind pressure $P_{sw} = n_{sw}m_p v_{sw}^2$. Here m_p is the mass of a proton. The IMF clock angle θ is given by $\tan^{-1}(B_y/B_z)$. The solar wind flow velocity v_{sw} is taken to be approximately the $v_x(t)$ component in GSM coordinates as measured by the solar wind monitor ACE.

The AL index is derived from measurement of the horizontal component of the Earth's magnetic field at stations located along the auroral arc in the Northern hemisphere. The AL index is compiled every minute over a 24 hour period in a day and is obtained by selecting the smallest values measured among 12 stations located along the Auroral zone, all of them above 50° latitude. The minimum values are taken to be the strongest activity of the westward auroral electrojet and here

it is compared to I_1 of the WINDMI model, the field aligned current (Region 1 FAC) that closes the electric current **j** in the nightside magnetosphere through the nightside auroral ionosphere. A scaling factor is allowed in the calculation of the prediction AL index from the model's $I_1(t)$ current. The method for determining this scaling factor is given in *Spencer et al., 2006* [20].

The Dst indices are obtained from the measurement of the Earth's magnetic field from observatories that are sufficiently distant from the auroral and equatorial electrojets and located at approximately $\pm 20^\circ$ latitude, while being evenly distributed in longitude. The Dst index is compared to the output from the WINDMI model through the ring current energy $W_{\rm rc}$ using the Dessler-Parker-Schopke relation [12].

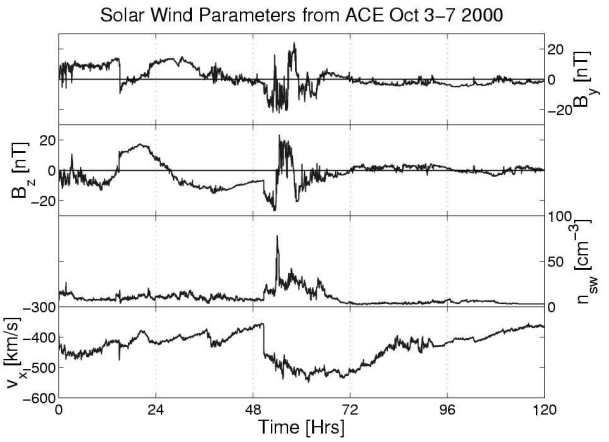

Fig. 1. ACE satellite measurement of the solar wind velocity v_x, proton density n_{sw}, IMF B_z and B_y components for October 3-7 2000, in GSM coordinates. The satellite was located at approximately $X = 224, Y = -29, Z = -5$ Earth radii in GSM coordinates during this period. The data shows a magnetic cloud from 3 October at 10:18 UT through 5 October at 05:34 UT and an IP shock at 02:40 UT on 5 October. On 3 and 4 October the AL index shows the occurrence of sawtooth oscillations, during the growth phase of the storm.

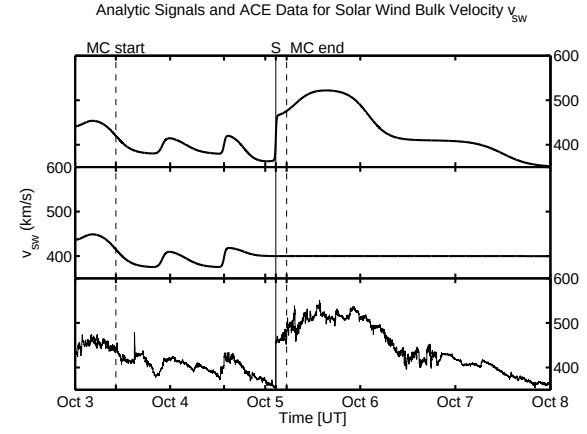

Fig. 2. Analytic input signal for v_{sw}, solar wind bulk velocity .

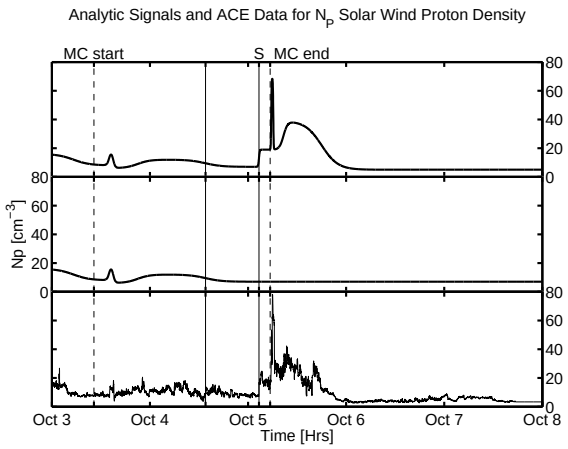

Fig. 3. Analytic input signals for the proton density N_p.

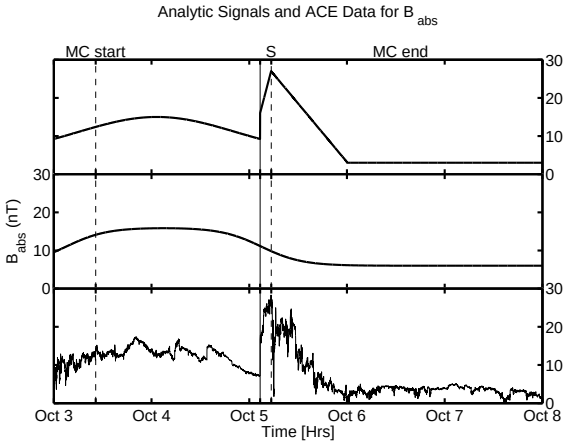

Fig. 4. Analytic input signals for the magnetic field magnitude $B_\perp$. The signals for all of the input fields for WINDMI from ACE solar wind data are shown in the above three figures. Top graphs: Analytic input signals for WINDMI. Middle Graphs: Analytic signals with removed shock features. Bottom graphs: Corresponding 3-6 October 2000 ACE data. MC shows where the magnetic cloud starts and stops. S denotes the location of the shock.

2.1. 3-6 October 2000

Figure 1 shows ACE observations for this storm. This event included a fast forward shock advancing into a preceding magnetic cloud [21]. ACE data shows a magnetic cloud from 3 October at 10:18 UT through 5 October at 05:34 UT lasting about 42 hours. The signature of the magnetic cloud can be seen from the plots of IMF B_y and B_z in Figure 1 as sinusoid-like waveforms, the IMF clock angle changes linearly through an angle of 180° through this period. The fast forward shock occurs at 02:40 UT on 5 October with a calculated shock speed of 534 km/s and compression ratio of 2.3. There are jumps in the velocity from 364 km/s to 460 km/s, the proton density from 7 $\rm cm^{-3}$ to 16 $\rm cm^{-3}$, and perpendicular magnetic field from 7 nT to 16 nT across the shock front.

The AL data shows a first large spike with a peak of -1938 nT occurring at 0651 UT on 5 October 2000. A second, larger spike of approximately -2790 nT in the AL index occurrs at

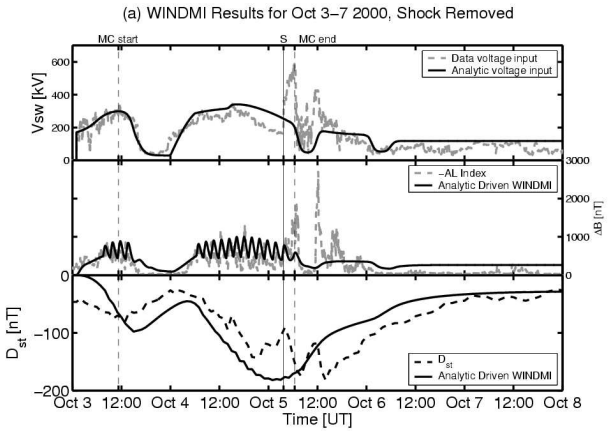

Fig. 5. WINDMI results: (a) The shock is removed from all analytic input signals.

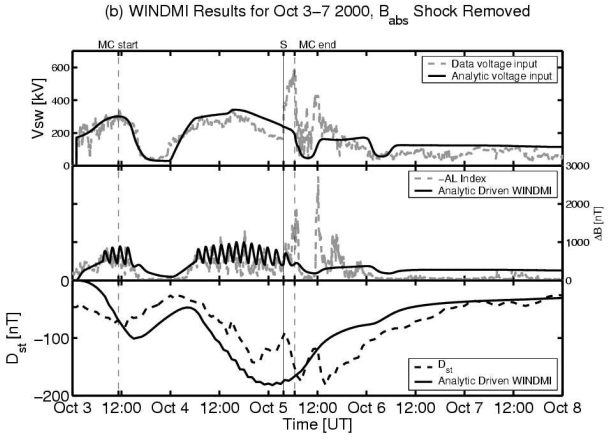

Fig. 6. WINDMI results: (b) The shock is removed from $B_\perp$ only.

1210 UT on 5 October 2000 initiated by a strong southward IMF excursion detected at ACE about an hour earlier. The Dst minimum of -180 nT is reached on 5 October slightly after the strong southward IMF surge.

Detailed analysis of the ACE data driven WINDMI results is given in [20] and [11]. These data driven results for the Dst and AL are compared to the analytic signal driven WINDMI results. The analytic signals based on the ACE data were constructed using hyperbolic tangent, gaussian, and linear functions. To study the role of the shock, the shock feature is removed from the solar wind parameters individually. In order to remove the shock feature from the analytic signals it was assumed that the parameter values would remain the values upstream of the shock. To compute an analytic driving voltage, signals for solar wind velocity v_{sw}, proton density N_p, magnetic field B_z, $B_\perp$, and clock angle θ were created. In Figures 2-4 the analytic solar wind parameters of solar wind velocity, proton density, and magnetic field are shown with and without the shock along with the corresponding ACE data.

The solar wind driving voltage was calculated using Equation 1 with our analytic signals with and without the shock feature. Using this input solar wind driving voltage the WINDMI model output was compared with and without the shock. In

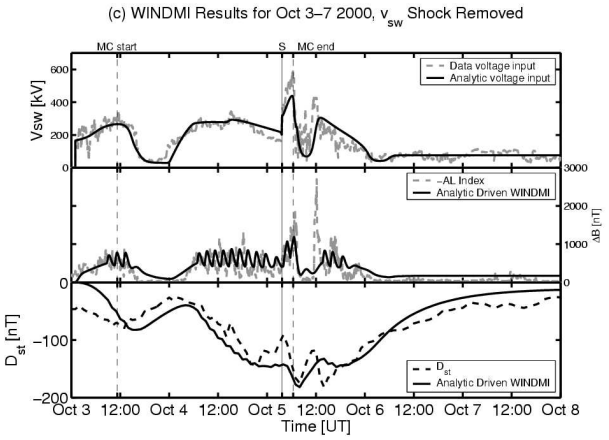

Fig. 7. WINDMI results: (c) The shock is removed from V_{sw} only.

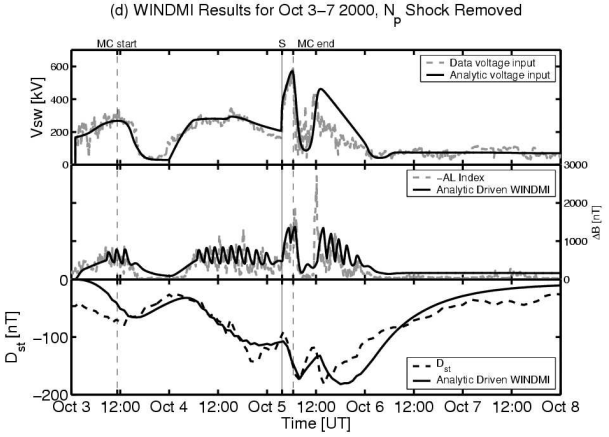

Fig. 8. WINDMI results for the AL (middle panel) and Dst (bottom panel) when (d) the shock is removed from N_p only when computing the solar wind driving voltage V_{sw} (top panel).

Figure 2 the shock feature is dropped from the solar wind velocity v_{sw} at ACE, the second AL peak (5 Oct 1200 UT) is lost due to the decreased solar wind driving voltage. In Figure 2 the shock is dropped from N_p we see an increase in both AL peaks (5 Oct 0700 and 1200 UT) due to an increased solar wind driving voltage. In Figure 2 the jump in $B_\perp$ is dropped both AL peaks (5 Oct 0700 and 1200 UT) decrease by 40% and 70% respectively, due to significantly decreased driving voltage. When the shock is dropped from all three parameters the result shown in Figure 2 is identical to removing the shock from $B_\perp$ only. These results show that the first large AL spike with a peak of -1938 nT occurring at 0720 UT 5 October 2000 was triggered by the shock front, and most strongly by the jump in $B_\perp$.

2.2. 15-24 April 2002

We have begun a similar analytic signal analysis for this storm period. ACE data during this period shows three fast forward shock events which are associated with halo CMEs observed in SOHO/LASCO. The first shock event occurred during the main phase of the storm and was observed by ACE

at 1020 UT on 17 Apr moving at a calculated shock speed of 480 km/s and is associated with a halo CME observed by SOHO/LASCO at 0350 UT moving at 720 km/s [16]. This CME is observed by ACE as a MC beginning at the start of 18 Apr and continuing until approximately 0200 UT 19 Apr. The next shock event occured during the main phase of the storm at 0801 UT on 19 Apr moving at a calculated speed of 650 km/s and is associated with a halo CME leaving the Sun at 0826 on 17 Apr moving at 1240 km/s [2]. This MC possibly produced the complex structure observed by ACE from 20-21 Apr. The third shock event occurred during the recovery phase at 0413 UT on 23 Apr moving at a calculated speed of 680 km/s and is associated with a non-geoeffective [22] halo CME leaving the Sun at 0127 UT on 21 Apr at a speed of 2393 km/s.

The shock analysis of this storm with the WINDMI model is ongoing but gives results consistent with those given in Section 2.1 for October. The jump in $B_\perp$ is the dominant source for the spikes in the AL index.

3. Real-time WINDMI

Real time measurements of the solar wind bulk velocity (V bulk), proton number density (Np), and the interplanetary magnetic field (Bx, By, Bz in GSM) are available from the Advanced Composition Explorer (ACE) satellite. These quantities are used to derive an input solar wind driving voltage for the WINDMI model. The rectified driving voltage is calculated in realtime using $V_{sw} = v_{sw} B_s^{IMF} L_y^{eff}$ where v_{sw} is the x-directed component of the solar wind velocity in GSM coordinates, B_s^{IMF} is the southward IMF component and L_y^{eff} is an effective cross-tail width over which the dynamo voltage is produced.

The WINDMI real time prediction of the AL and Dst indices is updated every 10 minutes for 2 day periods. Every 10 minutes the ACE data is automatically downloaded, formatted, and missing data points are replaced by the data point just before. From this data the solar wind driving voltage is calculated from both the rectified method and the Siscoe formula given in Equation 1. Currently the model is taking the rectified voltage as input, but this can be switched to the Siscoe driver at any time for comparison. Using this input, the WINDMI model runs every 10 minutes for the last 48 hour period with nominal parameters (parameters which have not been optimized for a particular storm) and outputs the AL and Dst prediction. The output is shown as a series of plots on the website[1], which show real time ACE data, the calculated driving voltage, the WINDMI AL and Dst, and real time AL and Dst data. There is also an email alert system set up which sends a notifiation when Dst activity is predicted below -50 nT or AL activity above 500 nT.

WINDMI predictions are compared to near realtime quicklook Dst data available the World Data Center for Geomagnetism, Kyoto University (also downloaded automatically every 10 minutes). WINDMI predicts the Dst index about two hours before the near realtime data is available from WDC Kyoto. WDC Kyoto also provides real time quicklook AE index data in the form of daily plots. WINDMI predicts the AL index about one hour before the data is available from WDC Kyoto.

[1] http://orion.ph.utexas.edu/∼windmi/realtime/

3.1. First Results: 14-15 April 2006

The first example of captured substorms by the real-time WINDMI model was on 14-15 April 2006. There were two storms on 5 April and 9 April leading up to 14 April, both with Dst minima around -100 nT. In Figure 9 the downloaded ACE real time solar wind data for this period is shown, including the calculated driving voltages. During this period the Dst reached a minimum of -122 nT at ∼0900 UT on 14 April and the AL index showed several large peaks from -1000 to -1500 nT. ACE data shows a magnetic cloud at the beginning of 14 April until about 1200 UT and from 14 - 15 April the solar wind bulk velocity was on the order of 600 km/s.

In Figure 10 the resulting AL and Dst predictions are shown in the bottom two panels. The WDC Kyoto real time Dst index is also plotted on the WINDMI Dst prediction plot. During most of the initial phase of the storm, from 14 April 0000 - 0700 UT, the Dst prediction underestimates the data by 30 - 70 nT. By the end of the initial phase the prediction is within 30 nT of the data. During the main phase between 0700 - 1500 UT 14 April, the prediction overestimates the Dst by about 20 nT and is about two hours behind. The prediction follows the Dst by 20 - 30 nT throughout the recovery phase.

The WDC Kyoto real time AE index is shown in Figure 11 in which the AL index shows a series of large peaks of about -1000 nT at 0600 UT, -1500 nT from 1000 - 1200 UT, and -1000 nT from 1700 - 2000 UT on 14 April. The AL continues to oscillated until the end of 15 April up to -500 nT. The AL prediction captures some global oscillatory behavior and the peaks of -1000 nT and -1500 nT on 14 April and more peaks up to -500 nT on 15 April.

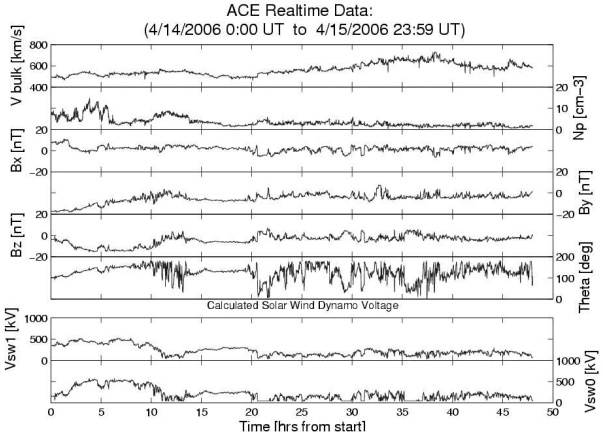

Fig. 9. Real-time solar wind parameters from ACE: Solar wind bulk velocity, proton density, Bx, By, Bz, and clock angle theta. Bottom panels show the solar wind driving voltage calculated by the Siscoe method (Vsw1) and rectified method (Vsw0).

3.2. Northward Turning Trigger

The northward turning trigger rules as discussed in [15] do not work for the October 2000 and April 2002 data. More complete rules have recently been proposed by Lyons at the ICS-8 conference. They have classified global auroral responses into a few fundamental response types, described as dynamic pressure, substorm, and null events [14]. When the IMF is not

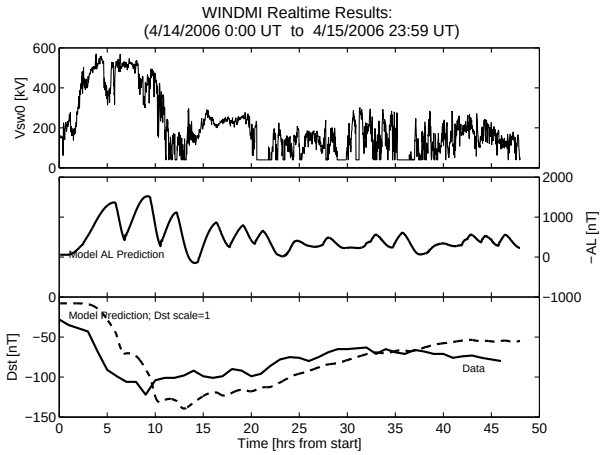

Fig. 10. Real-time WINDMI model predictions of AL (middle) and Dst (bottom) using the rectified driving volage (top) calculated in real-time as input. The Dst prediction is shown with a dotted line and follows the qualitative features of the data shown as with a solid line.

strongly southward but remains negative for about 30 minutes, and is followed by IMF changes leading to convection electric field reduction, typical substorms are observed. If it is instead followed by solar wind dynamic pressure enhancements, the magnetosphere is compressed which leads to global auroral enhancement without substorm bulge-region aurora or current wedge formation. When the IMF is strongly southward for a prolonged time and IMF changes lead to convection electric field reduction, this results in a typical substorm disturbance. For steady, strongly southward IMF conditions, the enhancement in the solar wind dynamic pressure causes compressive auroral brightening away from the bulge region and Harang-region substorm brightening. Null events are described as simultaneous IMF and dynamic pressure changes, which lead to a decrease in both E_y and B_{trans} in the inner plasma sheet, which prevents the occurrence of a substorm [14].

3.3. Future Work

The real-time WINDMI model can be broadened in two steps. The first step is to add the generalized northward turning trigger set of rules. An alarm would be sent with the type of condition violated and record the data for that 12 hour period. For future analysis, the second phase is building terms into the dynamical equations that represent the physical processes suggested by the northward turning models. In particular the weaknening of the ratio of transitional fields B_{trans} in the -6.6 to -10 R_E region and the strengthening of the convection electric field pressure in the central plasma sheet.

WINDMI and real-time WINDMI will be more useful when THEMIS (Time History of Events and their Macroscopic Interactions during Substorms) operates in real-time. THEMIS consists of five identical probes with orbits near the equatorial magnetotail to provide prolonged tail-aligned, crosstail and cross-sheet measurements. There will be in-situ particle and field measurements in addition to ground magnetometer network measurements of auroral onset [5].

Real-time WINDMI can be improved by including optimization of model parameters using a genetic algorithm, which has already been implemented for WINDMI [20]. The real-time version would update the optimized parameters every few hours based on the current parameters and recent magnetosphere conditions. Initial conditions can also be better determined by using the Local Ensemble Kalman Filter (LEKF) data assimilation scheme used in numerical weather models [13].

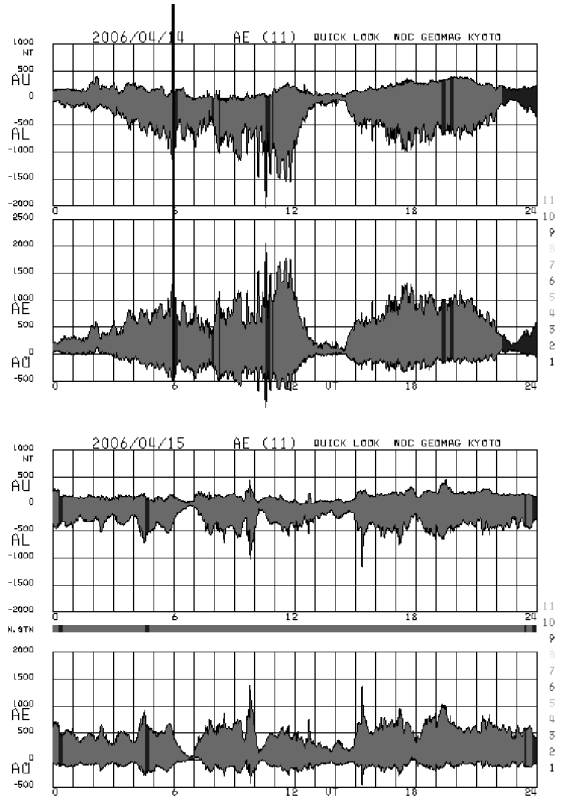

Fig. 11. AL data from WDC Kyoto for comparison. WINDMI AL prediction shown in Figure 10 captures the global features found in the data including the -1000 nT amd -1500 nT peaks on 14 April.

4. Summary

The effect of the IP shock events during the 3-6 October 2000 and 15-24 April 2002 geomagnetic storms on the AL and Dst indices were examined by the construction of analytic solar wind signals. WINDMI results from the analytic inputs show that the shock events impacted the AL index values but changed the Dst very little. In particular the the first large AL spike during the October storm was triggered by the shock front, and particularly by the jump in $B_\perp$.

The real-time WINDMI model collects ACE data every 10 minutes and outputs a prediction for the AL and Dst indices. The AL prediction is available one hour before any AL data is available, and for the Dst prediction this is two hours. Recently the real-time model captured a storm including substorms on 14-15 April 2006.

Acknowledgements

This work was partially supported by NSF grant ATM-0539099. The solar wind plasma and magnetic field data were obtained from ACE at NASA's CDAWeb site and the ACE Real Time Solar Wind site. The SOHO LASCO CME Catalog is generated and maintained by NASA and The Catholic University of America in cooperation with the Naval Research Laboratory. The geomagnetic indices used were obtained from the WDC for Geomagnetism, Kyoto.

References

1. L. Burlaga, E. Sittler, F. Mariani, and R. Schwenn, Magnetic loop behind an interplanetary shock - Voyager, Helios, and IMP 8 observations, *Journal of Geophysical Research, 86*, 6673–6684, 1981.
2. H. V. Cane, and I. G. Richardson, Interplanetary coronal mass ejections in the near-Earth solar wind during 1996-2002, *Journal of Geophysical Research, 108*, 6, 2003.
3. E. Echer, M. V. Alves, and W. D. Gonzalez, Geoeffectiveness of interplanetary shocks during solar minimum (1995-1996) and solar maximum (2000), *Solar Physics, 221*, 361–380, 2004.
4. E. Echer, and W. D. Gonzalez, Geoeffectiveness of interplanetary shocks, magnetic clouds, sector boundary crossings and their combined occurrence, *Geophysical Research Letters, 31*, 9808, 2004.
5. H. U. Frey, S. B. Mende, V. Angelopoulos, and E. F. Donovan, Substorm onset observations by IMAGE-FUV, *Journal of Geophysical Research, 109(A18)*, 10304, 2004.
6. W. D. Gonzalez, and B. T. Tsurutani, Criteria of interplanetary parameters causing intense magnetic storms (D_{st} < -100 nT), *Planetary and Space Sciences, 35*, 1101–1109, 1987.
7. J. T. Gosling, Coronal mass ejections and magnetic flux ropes in interplanetary space, *Washington DC American Geophysical Union Geophysical Monograph Series, 58*, 343–364, 1990.
8. J. T. Gosling, S. J. Bame, D. J. McComas, and J. L. Phillips, Coronal mass ejections and large geomagnetic storms, *Geophysical Research Letters, 17*, 901–904, 1990.
9. W. Horton, and I. Doxas, A low-dimensional energyconserving state space model for substorm dynamics, *Journal of Geophysical Research, 101(A12)*, 223-227, 1996.
10. W. Horton, and I. Doxas, A low-dimensional dynamical model for the solar wind driven geotail-ionosphere system, *Journal of Geophysical Research, 103(A3)*, 4561-4572, 1998.
11. W. Horton, E. Spencer, I. Doxas, and J. Kozyra, Analysis of the October 3-7 2000 GEM Storm with the WINDMI Model, *Geophysical Research Letters, 31*, L22102, 2005.
12. Introduction to Space Physics, edited by M.G. Kivelson and C.T. Russell, Cambridge Univ. Press, 1995.
13. D. Kuhl, I. Szunyogh, E. J. Kostelich, D. J. Patil, G. Gyarmati, M. Oczkowski, B. R. Hunt, E. Kalnay, E. Ott, and J. A. Yorke, Assessing Predictability with a Local Ensemble Kalman Filter, *Journal of the Atmospheric Sciences*, submitted, 2006.
14. L. R. Lyons, D.-Y. Lee, C.-P. Wang, and S. B. Mende, Global auroral responses to abrupt solar wind changes: Dynamic pressure, substorm, and null events, *Journal of Geophysical Research, 110(A9)*, 8208, 2005.
15. G. T. Blanchard, L. R. Lyons, and J. Spann, Predictions of substorms following northward turnings of the interplanetary magnetic field, *Journal of Geophysical Research, 105(A1)*, 375-384, 2000.
16. P. K. Manoharan, N. Gopalswamy, S. Yashiro, A. Lara, G. Michalek, and R. A. Howard, Influence of coronal mass ejection interaction on propagation of interplanetary shocks, *Journal of Geophysical Research, 109(A18)*, 6109, 2004.
17. D. M. Ober, N. C. Maynard, and W. J. Burke, Testing the Hill model of transpolar potential saturation, *Journal of Geophysical Research, 108*, 1467, 2003.
18. G. L. Siscoe, N. U. Crooker, and K. D. Siebert, Transpolar potential saturation: roles of region-1 current system and solar wind ram pressure, *Journal of Geophysical Research, 107(A10)*, 1321, 2002.
19. G. L. Siscoe, G. M. Erickson, B. U. O. Sonnerup, N. C. Maynard, J. A. Schoendorf, K. D. Siebert, D. R. Weimer, W. W. White, and G. R. Wilson, Hill model of transpolar potential saturation: comparisons with MHD simulations, *Journal of Geophysical Research, 107(A6)*, 1075, 2002.
20. E. Spencer, W. Horton, M. L. Mays, I. Doxas, and J. Kozyra, Analysis of the October 3-7 2000 and April 15-24 2002 Geomagnetic Storms with an Optimized Nonlinear Dynamical Model, *Journal of Geophysical Research*, submitted, 2006.
21. Y. M. Wang, P. Z. Ye , S. Wang, and X. H. Xue, An interplanetary cause of large geomagnetic storms: Fast forward shock overtaking preceding magnetic cloud, *Geophysical Research Letters, 30(13)*, 2003.
22. X. P. Zhao, and Y. Liu, Source Regions and Storm Effectiveness of Earth-Directed Halo CMEs Between 14 and 24 April 2002, *AGU Fall Meeting Abstracts*, 2003.